Applied Energy 363 (2024) 123047

Contents lists available at ScienceDirect

Applied Energy

journal homepage: www.elsevier.com/locate/apenergy

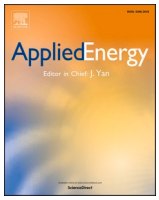

Innovative design for thermoelectric power generation: Two-stage thermoelectric generator with variable twist ratio twisted tapes optimizing maximum output

Wenlong Yang [a,b], Chenchen Jin [b], Wenchao Zhu [a,c], Changjun Xie [a,b,*], Liang Huang [b], Yang Li [d], Binyu Xiong [b]

[a] Hubei Key Laboratory of Advanced Technology for Automotive Components, Wuhan University of Technology, Wuhan 430070, China
[b] School of Automation, Wuhan University of Technology, Wuhan 430070, China
[c] State Key Laboratory of Advanced Technology for Materials Synthesis and Processing, Wuhan University of Technology, Wuhan 430070, China
[d] Department of Electrical Engineering, Chalmers University of Technology, Gothenburg 41258, Sweden

HIGHLIGHTS

- Two-stage thermoelectric modules boosts power output.
- Variable twist ratio twisted tapes to boost thermal energy extraction efficiency.
- Impact of tape pitch ratio and variable twist ratio on thermoelectric performance.
- Optimized thermoelectric generator net output power doubled.

ARTICLE INFO

Keywords:
Two-stage thermoelectric generator
Variable twist ratio
Twisted tape
Waste heat recovery
Heat transfer enhancement

ABSTRACT

In recent years, considerable effort has been dedicated to the development of highly efficient thermoelectric generators for waste heat recovery and thermoelectric power generation. In this study, we present employing twisted tapes with variable twist ratio to enhance thermal energy extraction efficiency, coupled with two-stage thermoelectric modules for heat-to-electricity conversion, resulting in a substantial increase in the power output of the thermoelectric generator. We established an experimental system that validated the superior power generation and heat recovery characteristics of the two-stage thermoelectric generator. Building upon these findings, we propose further optimizing the variable twist ratio twisted tapes to enhance the power output. We investigated the impact of tape pitch ratio, twist ratio, and twist ratio variation range on thermoelectric performance. Experimental results indicate that the influence of flow instability is more pronounced than that of swirl intensity, and twist tapes with the maximum twist ratio variation rate yield the highest net output power. Compared to an unmodified thermoelectric generator, the two-stage thermoelectric generator employing twist tapes with a twist ratio increase from π to 3π achieves a maximum net output power gain of up to 100%. These findings provide a practical framework for integrating innovative power generation modules and optimized heat exchanger designs into the application of waste heat recovery thermoelectric generators, marking a significant advancement in the field of thermoelectric generators.

1. Introduction

Various energy-intensive processes, such as industrial activities and power generation, often result in the wasteful dissipation of excess heat, leading to a significant squandering of energy and resources. Waste heat recovery, a pivotal research domain garnering global attention, presents an avenue for enterprises to diminish energy consumption, carbon emissions, and costs. The conversion of waste heat into efficient electrical power is considered among the most optimal techniques for waste heat utilization, given the substantial volume of waste heat, where even marginal advancements may yield profound changes [1].

* Corresponding author at: Hubei Key Laboratory of Advanced Technology for Automotive Components, Wuhan University of Technology, Wuhan 430070, China.
E-mail addresses: wenlongyang@whut.edu.cn (W. Yang), jackxie@whut.edu.cn (C. Xie).

https://doi.org/10.1016/j.apenergy.2024.123047
Received 30 December 2023; Received in revised form 23 February 2024; Accepted 15 March 2024
Available online 23 March 2024

Nomenclature

c_p	specific heat capacity, W/(m^2•K)
H	pitch length, m
I	current, A
L	tape distance, m
m	mass flow rate, g/s
P	power, W
Q_h	hot end heat flow, W
R_L	load resistance, Ω
T	temperature, K
U	voltage, V
V	volume flow rate, m^3/h
W	tape width, m
Δp	pressure drop, Pa
ΔT	temperature difference, K

Greek symbols

η	efficiency, %
ρ	density, g/m^3
σ	maximum error

Subscript

out	output value
p	pumping value
net	net value
ex	exhaust gas
te	thermoelectric element
hr	heat recovery
in	inlet value
out	outlet value
max	maximum value

Abbreviations

TEG	thermoelectric generator
TEM	thermoelectric module
ITR	increasing twist ratio
DTR	decreasing twist ratio
TR	twist ratio
PR	tape pitch ratio
TT	twisted tape

Thermoelectric Generators (TEGs) emerges as a promising green waste heat recovery technology, directly transforming thermal energy into electricity. Thermoelectric generators possess unique advantages such as solid-state conversion, absolute noiselessness, low maintenance costs, and structural simplicity [2]. The solid-state conversion is achieved through Thermoelectric Modules (TEMs), utilizing the Seebeck effect to directly convert temperature differentials into electrical energy. Research on waste heat TEGs has been extensively documented, primarily concentrated in the domains of automotive and marine engines [3].

Despite the increasing prevalence of electric vehicles [4], fossil fuel-powered automobiles emit substantial waste heat through their exhaust systems. Due to the limitations of Carnot cycle efficiency, this results in energy wastage and environmental issues. Even a modest proportion, such as 6%, converted into electricity could reduce fuel consumption by 10% [5], offering numerous benefits to both the environment and energy efficiency. Hence, efficient recovery of vehicle waste heat is imperative to reduce emissions and enhance energy efficiency. Liu et al. [6] installed four TEGs on an off-road vehicle, achieving a maximum output power of 944 W through road tests and dynamometer experiments. Zhang et al. [7] employed a TEG constructed with nanostructured materials for recovering waste heat from automotive diesel engines, achieving 1 kW of electricity production with a thermoelectric efficiency of 2.1%. These studies underscore the feasibility and vast application prospects of thermoelectric generators for vehicle waste heat recovery. However, the generation of such significant electrical power comes at the cost of exacerbated weight and economic considerations [8]. Substantial improvements in power density, economic viability, and conversion efficiency are necessary to effectively promote the widespread application of automotive thermoelectric generators.

Researchers are diligently enhancing the performance of TEGs from multiple perspectives, encompassing the development of novel thermoelectric materials [9], innovative thermoelectric module structures [10], optimization of circuit topologies [11], augmented heat transfer at the hot end [12], and optimization of heat dissipation [13]. Through these investigations, fundamental parameters governing the performance of exhaust waste heat recovery TEGs have gradually come to light. Constrained by the low conversion efficiency of current commercial thermoelectric materials (below 5%), achieving 20 W of electricity from a single TEM necessitates the passage of at least 400 W of heat at the hot end [14]. This is attributed to the fact that, aside from the intrinsic thermoelectric conversion capability of the material itself, the power generation is contingent upon the temperature differential at both ends. However, due to the remarkably limited convective heat transfer coefficient at the gas-solid interface, collecting a heat flow exceeding 400 W for each TEM proves to be particularly challenging [1]. Consequently, the heat exchange between the gas and the thermoelectric module emerges as a pivotal factor determining the performance of thermoelectric generators for exhaust waste heat recovery, constituting one of the foremost challenges in the current landscape [15].

Through extensive research, researchers have gradually identified solutions to the issue. A commonly employed method is optimizing the arrangement of internal heat exchangers, aiming to minimize the thermal resistance of the exchangers. The desired outcome is the reduction of the temperature differential between the hot gas and the thermoelectric module surface, ultimately achieving the goal of enhancing the heat extraction rate and power generation. One of the simplest and most effective approaches to optimize the heat exchanger arrangement involves the insertion of flow disturbance elements [16]. He et al. [17] investigated the enhanced heat transfer effects of plate fin heat exchangers in the context of waste heat recovery TEGs from heavy-duty diesel engines. The results indicated that the spacing and height of the fins had a more significant impact than the thickness of the fins, although the study did not account for the influence of fins on exhaust pressure drop and net power. Pujol et al. [18] explored the thermoelectric and flow resistance characteristics of a single TEG under forced convection conditions, employing plate fins. They found that the net output power was less sensitive to changes in fin thickness than changes in fin spacing. Chen et al. [19] conducted a comparative study on the effects of pin fins and plate fins in enhancing TEG performance. They discovered that both pin fins and plate fins, compared to smooth pipes without fins, could multiply the output power of the thermoelectric module. Following numerical optimization, the output power of pin fins could be up to 24.14% higher than that of plate fins. Zhao et al. [20] investigated the impact of inserting perforated baffles into the heat exchanger on thermoelectric performance. They found that the optimal installation position could increase the output power by 73.4%, with exhaust temperature and flow rate having minimal influence on the optimal position.

Furthermore, filling the heat exchanger with foam metal not only maximizes the heat transfer coefficient but also improves the temperature uniformity along the TEG, alleviating the power mismatch issue to a

certain extent [21]. Li et al. [22] analyzed the performance of a thermoelectric generator with the insertion of porous foam copper in the central flow region of the heat exchanger. Compared to a thermoelectric generator without foam metal insertion, the output power of the TEG using high-porosity, high-volume-ratio porous foam copper could be increased by up to 2.3 times. However, the pressure drop would rise to over 10 kPa, posing significant negative impacts on the engine.

In addition to inserting various structures of flow disturbance devices in the ducts, enhancing the heat transfer between the gas and the thermoelectric module can also be achieved by improving the shape of the TEG's channels [23]. Luo et al. [24] proposed a convergent heat exchanger where the hot-side channels converge along the direction of fluid flow. The output power of the convergent TEG was 5.9% higher than that of a traditional flat-plate TEG. Addressing a circular heat source, Yang et al. [25] introduced a concentric circular thermoelectric generator, where the center of the hot-side channel was filled with a cylinder, reducing the fluid space and thereby increasing the heat transfer coefficient. Results indicated that, compared to a smooth heat exchanger, the net output power of the concentric circular TEG could increase by up to 65%. The commonality in these studies lies in reducing the cross-sectional area of fluid channels or increasing fluid turbulence to enhance the heat transfer coefficient. However, the improvement in heat transfer is often accompanied by deterioration in other aspects [26], such as friction coefficients. Currently, there is a lack of a widely accepted heat transfer enhancement method that can effectively increase the heat transfer coefficient while maintaining low pressure drop. Net power is typically used to represent the coupled effects of heat transfer enhancement in the TEG and the additional pressure drop. The extra pressure drop results in pumping power losses for the engine. Net power is generally the difference between TEG output power and pumping power.

Due to its excellent performance, light weight, simplicity of installation, and low manufacturing/operating costs, the insertion of twisted tapes (TTs) has recently become one of the most popular heat transfer enhancement devices [27,28]. Twisted tapes are typically made of metal, twisted into specific shapes and sizes, and inserted into the flow channels. They are also considered vortex generators, serving as turbulence inducers to convey vortex flow, resulting in an increase in the heat transfer coefficient. There have been few reports on the application of twisted tapes in TEGs.

Zhu et al. [29] inserted a typical TT into the circular tube heat exchanger of a annular TEG and optimized the key parameters of the tape using a genetic algorithm. The results showed that, compared to a smooth pipe, under the optimal tape structure, the net power and efficiency increased by 10.41% and 22.51%, respectively. They installed a twisted tape in the heat exchanger that were much smaller in diameter than the pipe, hence the improvement in TEG performance was not very pronounced. Researchers have conducted studies on heat transfer enhancement by inserting TTs in both circular and square tubes [30]. The results indicate that using TTs is an economical heat transfer enhancement solution. Moreover, due to the high aspect ratio of rectangular ducts, their heat transfer increment is higher than that of circular ducts. This suggests that twisted tapes in flat-plate heat exchangers can achieve better performance. Karana et al. [31] investigated the effects of different pitch ratios, helix angles, and twist ratios on the thermoelectric performance of a diesel engine TEG. The results showed that the optimal configuration was a pitch ratio of 8, a helix angle of 60°, and a twist ratio of 4, yielding the maximum net output power. At an engine speed of 1700 rpm and a torque of 60 N·m, the net power could be increased by 82% compared to a smooth heat exchanger. There is still further potential for improvement, as there have been extensive reports indicating that modifying the twisted tape can lead to better heat transfer performance [28].

In addition to enhancing heat transfer, improving the thermoelectric modules is an effective method to achieve higher power output within the limited volume constraints of a TEG [32]. To increase power density, a promising solution is the implementation of two-stage TEGs [33]. This configuration involves stacking two typical thermoelectric modules together, electrically connected in series or parallel, with typically only a ceramic layer serving as an insulator between them. Recently, research on two-stage thermoelectric modules has garnered increasing interest [34,35], as it allows for better electrical energy output within the same footprint. However, much of the research has been confined to numerical simulations and simulation analyses. In the context of exhaust waste heat recovery TEGs for internal combustion engines, there is a lack of experimental evaluation and validation of the thermoelectric properties of two-stage thermoelectric modules.

Table 1 summarizes recent experimental studies on TEGs used for internal combustion engine exhaust waste heat recovery. The table includes information on the thermoelectric module sizes, quantities, heat transfer enhancement measures, and the obtained output performance. From the table, it is evident that all studies discussed improvements in thermoelectric performance using single-stage thermoelectric modules. However, detailed experimental data on the performance of two-stage thermoelectric generators and twisted tape-enhanced heat transfer are still lacking, making reliable optimization studies challenging through numerical simulations.

This study differs from previous research in two aspects. Firstly, a two-stage thermoelectric module was manufactured and implemented to recover exhaust heat energy. Compared to typical thermoelectric modules, it allows for higher power output within the same footprint. Secondly, we inserted our proposed twisted tapes with variable-twist ratio in the heat exchanger to enhance heat transfer. This swirl-inducing device achieves better heat transfer enhancement. The study explores the impact of twisted tape configurations on the output power, conversion efficiency, pressure drop, net power, and heat recovery rate of a two-stage thermoelectric generator under different engine conditions. The results of this research will provide valuable guidance for the design and optimization of two-stage thermoelectric generators and twisted tape heat exchangers.

2. Experimental platform development

2.1. Configuration of two-stage TEG

The schematic representation of the TEG is illustrated in Fig. 1(a) and (b). It comprises a plate-type heat exchanger, two thermoelectric module layers, and four radiators. The channel thickness of the plate-type heat exchanger is 1.5 mm, with dimensions of 320 mm (length) × 120 mm (width) × 20 mm (height). Twenty-four two-stage thermoelectric modules are arranged in a 2 × 6 configuration at both ends of the heat exchanger, interconnected in series. Surrounding the outer surface of the thermoelectric modules are four radiators, each measuring 300 mm (length) × 50 mm (width) × 12 mm (height), covering every six TEMs with a cooling conduit. Apart from the TEMs, other principal components are constructed from aluminum alloy.

Two-stage thermoelectric modules were fabricated based on typical commercially available Bi_2Te_3-based TEM, as illustrated in Fig. 1(c) and (d). Under the condition of a hot-end temperature of 523 K, the parameters of a standard commercial single-stage thermoelectric module, provided by the supplier, are shown in Table 2. The external dimensions of the two-stage thermoelectric module are 50 mm (length) × 50 mm (width) × 6.8 mm (height). This two-stage thermoelectric module consists of upper and lower parts, with each level comprised of 198 *p*-type or *n*-type thermoelectric legs (each measuring 1.4 mm in length, 1.4 mm in width, and 1.6 mm in height) connected in series between 0.3 mm thick copper electrodes. In total, there are 396 semiconductor legs, forming 198 pairs of *pn* thermocouples. The outer surface of the two-stage module and the intermediate region between the two stages are insulated by 0.8 mm thick Al_2O_3 insulating plates. The Seebeck coefficient and resistivity are approximately ±190–230 μV/K and 0.85 mΩ·cm, respectively. Considering the thermal properties of the solder used for

Table 1
Recent experimental studies on exhaust heat recovery TEGs for internal combustion engines.

TEM structure	TEM quantity	TEM size (length × width × height)	Methods to enhance heat transfer	Maximum output power	Maximum efficiency	Pressure drop	Ref.
Single-stage	24	40 × 40 × 3.3 mm^3	Staggered pin fins	96.6 W	3.95%	0.37 kPa	[14]
Single-stage	8	55× 51.5 × 3.3 mm^3	Partially filled with copper foam	36 W	N/A	5.4 kPa	[22]
Single-stage	20	56× 56 × 5.5 mm^3	Typical twisted ribs	94.7 W	N/A	N/A	[31]
Single-stage	40	44 × 44 × 3.6 mm^3	Stainless steel perforated plates and plate fins	119 W	2.8%	1.4 kPa	[36]
Single-stage	10	55× 55 × 4 mm^3	Rectangular winglet longitudinal vortex generators	7.1 W	1.1%	N/A	[37]
Single-stage	40	50 × 50 × 3.8 mm^3	Smooth flat heat exchanger (4 mm in height)	29.5 W	1.25%	0.12 kPa	[38]
Single-stage	30	60 × 60 × 3.3 mm^3	Flow straightener and plate fins	83 W	2.5%	1.9 kPa	[39]
Single-stage	18	40 × 40 × 3.6 mm^3	Conical heat exchanger structure with perforated plate and fin	98.8 W	2.6%	2.05 kPa	[40]
Single-stage	32	40 × 40 × 3.3 mm^3	Porous copper foam	5.8 W	2.05%	0.81 kPa	[41]

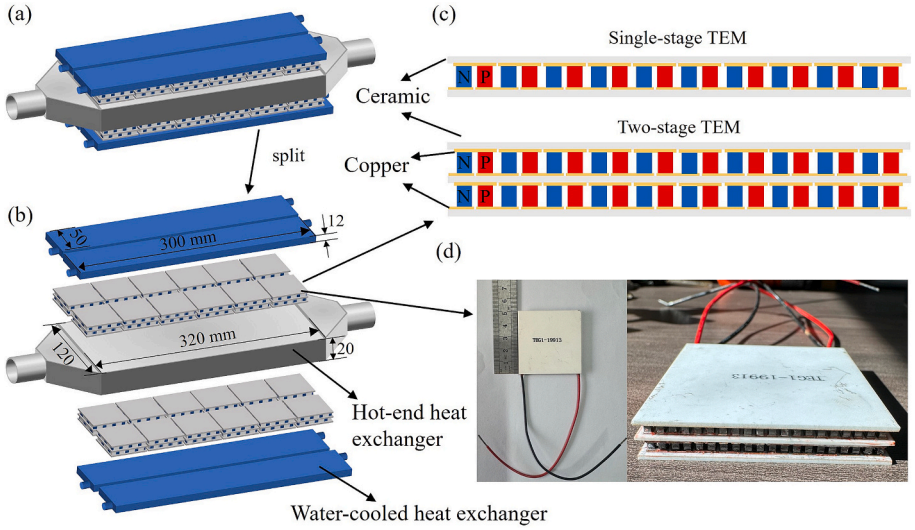

Fig. 1. (a) TEG structure diagram. (b) TEG structure splitting diagram. (c) Two-dimensional diagrams of single-stage and two-stage TEM. (d) Manufactured two-stage TEM.

Table 2
Parameters of single-stage TEM (TEG-19913).

Parameters	Cold end temperature	
	300 K	323 K
Open-circuit voltage (V)	13.0	11.8
Dynamic internal resistance (Ω)	2.8	2.9
Maximum output power (W)	14.5	11.5
Conversion efficiency (%)	5.7	5.0
AC internal resistance (Ω, 297 K)	1.58	1.58

connecting the thermoelectric legs to the copper electrodes and the optimal ZT temperature range of BiTe materials, the maximum allowable surface temperature is 523 K.

2.2. Twisted tape with variable twist ratio

The installation of twisted tapes is exceedingly straightforward, accomplished through the insertion into the pipeline. To facilitate the insertion of the helical tapes, the width (W) of the tapes must align with the height of the pipeline [28], ensuring a secure fastening within the heat exchanger channels. When replacement becomes necessary due to maintenance, structural upgrades, or other reasons, the inserted tapes can be easily retracted. Following modification, the same installation method, as described earlier, can be maintained. In this investigation, all tested twisted tape inserts are crafted from aluminum, possessing a width of 20 mm, a length of 300 mm, and a thickness of 1 mm.

The pitch length and twist ratio directly influence the performance of the twisted tape. The pitch length (depicted in Fig. 2) typically refers to the length (H) of the tape that undergoes a 180° rotation, used in calculating the twist ratio. The Twist ratio (TR) determines the twisting frequency of the tape and is calculated as the ratio of pitch length to tape radius (TR = H/R). Furthermore, within the internal structure of a flat-type heat exchanger, multiple tapes can be inserted since multiple-twist tapes yield higher heat transfer rates compared to single-twist tapes [42]. The distance between adjacent tapes, denoted as L, defines the density of the twisted tape inserts within the finite heat exchanger channel, represented by the tape pitch ratio (PR = L/W). Fig. 2 illustrates the key parameters of the twisted tapes studied in this research.

Twisted tapes have the capacity to generate heightened heat transfer rates, albeit at the cost of increased frictional losses. To strike a more

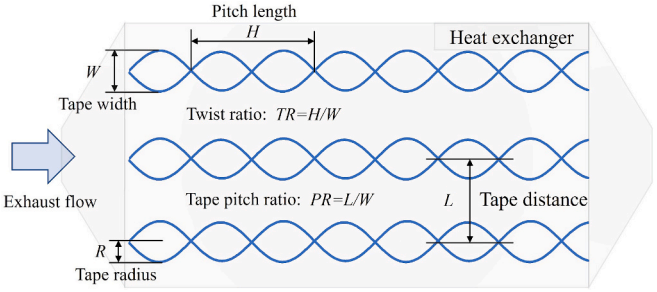

Fig. 2. Key parameters of twisted tapes.

favorable balance between enhanced heat transfer rates and augmented pressure losses, refinement of the twisted tape design is imperative. In the case of exhaust gas waste heat recovery systems where a significant temperature gradient is prevalent along the flow direction of the channels, the distinct temperature gradients induce uneven potential distribution across the series-connected TEMs, resulting in parasitic power losses [43]. Therefore, the objective of this study is to ameliorate this scenario and seek the most efficient heat transfer enhancement measures while maintaining a lower pressure drop. A novel twisted tape structure is proposed, characterized by a variable pitch along the length of the tape. In three-dimensional space, the structure of the twisted tape can be represented by the following expression:

$$\begin{cases} x = R{\cdot}cos\left(\dfrac{2\pi}{W{\cdot}TR}t\right) \\ y = R{\cdot}sin\left(\dfrac{2\pi}{W{\cdot}TR}t\right) \\ z = t \end{cases} \tag{1}$$

where t = [0,300].

To construct a twisted tape with variable twist ratio, one simply needs to linearly increase or decrease 2π/(W·TR). When the TR gradually decreases along the fluid flow direction, it is termed as a decreasing twist ratio twisted tape (DTR-TT); conversely, when the TR gradually increases along the fluid flow direction, it is designated as an increasing twist ratio twisted tape (ITR-TT).

For a standard constant twist ratio twisted tape, a general trend suggests that as the pitch length decreases, thermodynamic performance increases. This relationship exhibits an optimal point where the increase in frictional losses and the improvement in convective heat transfer reach an optimal balance. Traditionally, researchers often adopt "6" as the optimum TR value [30]. In the realm of variable twist ratio twisted tapes, it can be perceived as a compromise value, wherein variations in pitch are explored based on TR = 6, investigating the performance of variable twist ratio twisted tapes under different combinations. According to the expression for variable twist ratio tapes, Eq. (1), its TR alteration is associated with π. Consequently, we have devised specific specifications of variable twist ratio twisted tapes based on π, 2π, and 3π as TR boundaries. Fig. 3 illustrates schematic diagrams of typical constant twist ratio twisted tapes and variable twist ratio twisted tapes.

To handle the structural characteristics of variable twist ratio twisted tapes in a dimensionless manner, we define the variable twist ratio parameter (VTR) as the ratio of the twist ratio at the beginning to that at the end of the tape. Thus, for three types of increasing twist ratio twisted tapes, VTR = 1/3, 1/2, and 2/3, while for three types of decreasing twist ratio twisted tapes, VTR = 3/2, 2, and 3. This definition can be extended to variable twist ratio twisted tapes with different structural parameters, where VTR < 1 signifies increasing twist ratio twisted tapes, VTR = 1 denotes conventional constant twist ratio twisted tapes, and VTR > 1 indicates decreasing twist ratio twisted tapes. As VTR approaches 1, the rate of twist variation diminishes, whereas it increases as VTR deviates further from 1.

2.3. Apparatus and experimental settings

The fabricated two-stage TEMs were integrated with the variable twist ratio twisted tapes into the TEG experimental system for the assessment of thermoelectric performance. By designing the physical structure of the variable twist ratio twisted tapes in three-dimensional software and subsequently employing metal 3D printing technology, we fabricated the DTR-TT and ITR-TT. The experimental system consists of an air heating system, TEG, a cooling water circulation system, an electronic load, and a data acquisition system (Fig. 4).

The air heating system utilizes an industrial hot air blower (RY-P-15 A-075) as a simulated heat source, replacing an automobile engine, to steadily provide the required flow and temperature of high-temperature gas [24]. The industrial hot air blower comprises a blower, a heater, and a control circuit. With a maximum power of 15 kW, the industrial hot air blower draws in ambient air and heats it. The exhaust temperature can be adjusted within the range of 300–633 K with a PID controller (accuracy ±0.5 K). The outlet flow rate of the hot air blower can be regulated within the range of 0–240 m^3/h by adjusting the control panel.

Section 2.1 has provided a detailed description of the customized TEG, with a detachable side of the hot-end heat exchanger, allowing the

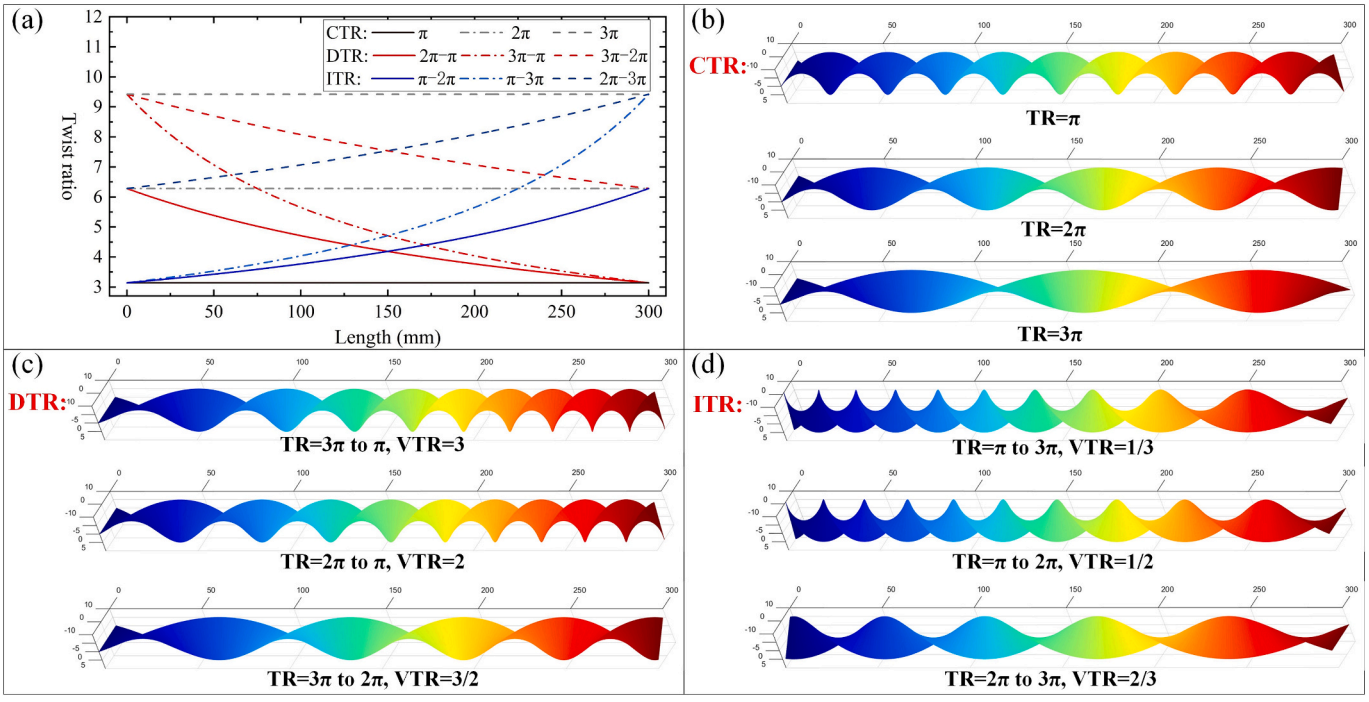

Fig. 3. (a)Variations of the twist ratio along the length and schematic diagrams of (b) constant twist ratio, (c) decreasing twist ratio and (d) increasing twist ratio of the twisted tapes.

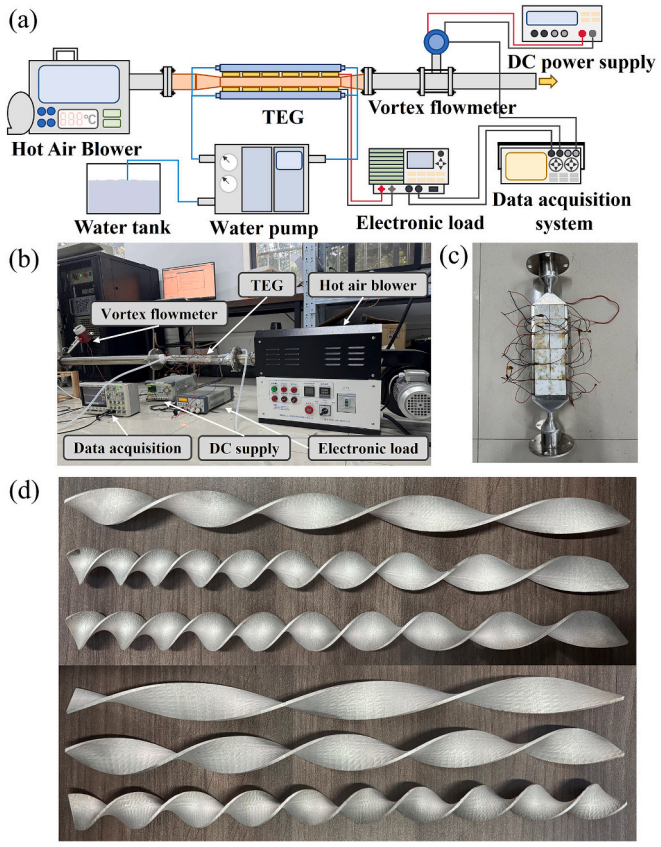

Fig. 4. Experimental configuration.

insertion of the twisted tape. The TEG is connected to the industrial hot air blower via flanges. To minimize thermal resistance, the contact surfaces between the heat exchanger, thermoelectric modules, and radiators are coated with thermally conductive silicone grease. Bolts are applied on both sides of the TEG for secure fastening.

The cooling water circulation system primarily consists of a water tank, a water pump, and pipelines. A chilling unit (SHZ-95B) pumps cold water from a 50 L water tank through the cold-side heat exchanger of the TEG, maintaining a low temperature on the cold side of the TEG. The output flow rate of the chilling unit is approximately 10 L/min, connected to four radiators in the TEG system via rubber hoses. Due to the large capacity of the cooling water tank, the cooling water temperature remains nearly constant during the experimental process, achieving stable output shortly after starting the TEG.

The electronic load and data acquisition system include a vortex flowmeter, a DC power supply unit, an electronic load, and a data acquisition instrument. To measure the actual exhaust outlet flow rate, temperature, and heat exchanger outlet pressure, a vortex flowmeter (HW-LUGA14, full range 50– 480 m^3/h, accuracy ±1%) is installed at the outlet of the heat exchanger. A 24 V DC power supply (RIGOL DP832) powers the vortex flowmeter. An electronic load (Array 3721 A, resolution 0.1 mΩ, accuracy ±0.5%) is connected to the thermoelectric modules to simulate external load conditions. All experimental data, including the TEG's output current, temperature, and pressure, are measured and collected using a data acquisition device (Agilent DSO-X 2024 A).

The hot air blower, TEG, and vortex flowmeter are connected using stainless steel pipes with flanges. The hot fluid output from the hot air blower flows through the TEG and vortex flowmeter, discharging into the environment. Furthermore, during the experimental process, the TEG is enveloped in silicone felt with an extremely low thermal conductivity to minimize heat losses. Given the direct connection between the hot air blower and the TEG, the temperature at the outlet of the blower is considered as the inlet temperature of the TEG. This temperature measurement is facilitated by sensors and controllers integrated within the blower. The outlet temperature is directly measured via the vortex flowmeter. The flow velocities at the TEG's inlet and outlet are directly measured by the hot air blower and the vortex flowmeter, respectively. The inlet pressure of the TEG is estimated by referencing the performance curve provided by the manufacturer of the hot air blower. This curve delineates the relationship between outlet pressure, airflow velocity, and power under various operating conditions. The outlet pressure of the TEG is directly measured by the vortex flowmeter.

2.4. Experimental procedure

The power output and back pressure of the TEG are significantly influenced by the operational state of the engine. Kim et al. [36] conducted tests on a turbocharged six-cylinder diesel engine, recording operational parameters of the TEG system under various engine modes. The engine had a cylinder bore of 103 mm, a stroke of 118 mm, a compression ratio of 17:1, and a maximum power of 110 kW at 2500 rpm. Fig. 5 illustrates the impact of engine load on TEG inlet temperature and mass flow rate at different engine speeds. In the current study, to simulate the actual operating conditions of an automotive waste heat recovery TEG system, six typical vehicle operating conditions from Ref. [36] were considered, as shown in Table 3. During the experiments, the outlet temperature and flow rate of the industrial hot air blower were adjusted through the control panel to operate the TEG under specific engine exhaust conditions. Furthermore, the influence of vehicle speed on the entrance parameters of the cooling system is negligible [44].

In each run, the TEG initially operated in an open circuit. Firstly, the cooling water unit was activated to ensure the circulation of cooling water. Subsequently, the industrial hot air blower was turned on and adjusted to a fixed exhaust condition. After a period of operation, the outlet temperature of the TEG was dynamically measured, considering it in a steady state when the rate of change over five consecutive minutes was within ±0.2 K. Finally, the electronic load was connected to the TEM, and parameters such as TEG voltage, current, outlet pressure, and flow rate were measured and recorded.

2.5. Data analysis

In the experiment, as the industrial hot air blower is directly connected to the TEG, the outlet temperature of the blower is considered as

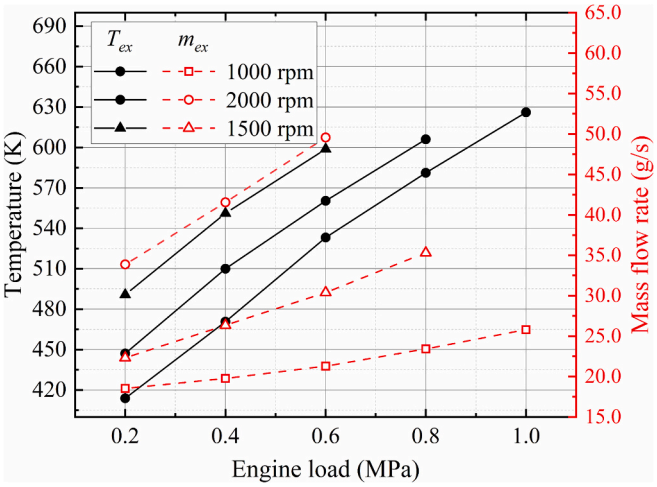

Fig. 5. Variations in exhaust temperature and mass flow rate with engine speed and load.

Table 3
Selected typical TEG operating conditions.

Engine mode	Engine Load (MPa)	Speed (rpm)	Mass flow rate (g/s)	Temperature (K)
A	0.4	1000	19.7	470.7
B	0.4	1500	26.3	509.9
C	0.4	2000	41.5	551.1
D	0.6	1000	21.3	533.1
E	0.6	1500	30.4	560.3
F	0.6	2000	49.5	598.8

the inlet temperature of the TEG ($T_{ex,in}$). The outlet temperature ($T_{ex,out}$) and volumetric flow rate (V_{ex}) of the TEG were measured using the vortex flowmeter. Therefore, the thermal energy extraction rate (Q_h) from the exhaust flow in the TEG region is calculated by the following Eq. [45]:

$$Q_h = m_{ex}c_{pex}\Delta T_{ex} = V_{ex}c_{pex}\Delta T_{ex}/\rho_{ex} \tag{2}$$

The maximum possible energy extraction rate can be obtained by using the atmospheric temperature as the reference temperature, as shown below:

$$Q_{h,max} = V_{ex}c_{pex}\Delta T_{ex,a}/\rho_{ex} \tag{3}$$

$$\eta_{hr} = Q_h/Q_{h,max} \tag{4}$$

where ΔT_{ex} represents the temperature difference of the exhaust at the TEG inlet and outlet, and $\Delta T_{ex,a}$ represents the difference between the exhaust temperature at the TEG inlet and the ambient temperature. The ratio of the actual energy extraction rate (Q_h) to the maximum possible energy extraction rate ($Q_{h,\max}$) indicates the thermal energy recovery efficiency η_{hr} of the TEG.

The output power (P_{out}) is dependent on the load resistance (R_L) and can be calculated by measuring the current (I) and voltage (U) across the load resistor. The calculation formula is as follows:

$$P_{out} = UI \tag{5}$$

The thermoelectric conversion efficiency η_{te} is expressed as:

$$\eta_{te} = P_{out}/Q_h \tag{6}$$

When applying a disrupter to the hot-end heat exchanger of the TEG, to calculate the back pressure power loss, according to [46], it can be computed as:

$$P_p = V_{ex}\Delta p = m_{ex}\Delta p/\rho_{ex} \tag{7}$$

where Δp is the pressure drop of the hot fluid through the heat exchanger, and ρ_{ex} is the density of the exhaust gas.

Therefore, the net output power (P_{net}) of the TEG is calculated as:

$$P_{net} = P_{out} - P_p \tag{8}$$

In addition, the measurement error is calculated based on the definition of heat transfer rate and the accuracy of each measurement sensor [38]. The specific equation is as follows:

$$Q_h = \sqrt{\left(\frac{\partial Q_h}{\partial V_{ex}}\sigma V_{ex}\right)^2 + \left(\frac{\partial Q_h}{\partial T_{ex,in}}\sigma T_{ex,in}\right)^2 + \left(\frac{\partial Q_h}{\partial T_{ex,out}}\sigma T_{ex,out}\right)^2} \tag{9}$$

where σ represents the maximum error of each measurement parameter. The calculated Q_h error is within ±3.17%. According to the above equation, the uncertainties of the output power, conversion efficiency, and pressure drop are calculated to be ±0.171%, ±3.181%, and ± 0.862%, respectively.

3. Results and discussion

3.1. Output performance of two-stage thermoelectric generators

Primarily, an examination was conducted within the smooth channel devoid of twisted tapes, exploring the electrical characteristics of single-stage TEG and two-stage TEG under varying external resistances. To quantitatively analyze power output, power-load resistance curves for the TEG system were obtained by altering external loads under diverse engine modes, as depicted in Fig. 6. Irrespective of whether it was a single-stage TEG or a two-stage TEG, the power output increased with escalating engine speed and load. Under engine mode F, the two-stage TEG outperformed the single-stage TEG, exhibiting a power output enhancement of 17.3%. The enhancement rate decreases with the increase of exhaust temperature and mass flow rate. This phenomenon arises because, despite the heightened temperature gradient between the cold and hot ends of the TEG, the enhancement in the operational temperature difference for both the upper-level and lower-level TEMs is not pronounced. For the single-stage TEG, characterized by lower internal resistance, the increase in temperature gradient yields a more conspicuous improvement in output power.

With the escalation of external resistance, the output power initially rises before diminishing. There exists an optimal load resistance, enabling the TEG to achieve peak output power. Furthermore, from Fig. 6, it is discernible that the operational mode of the engine significantly influences peak output power. The optimal load exhibits a

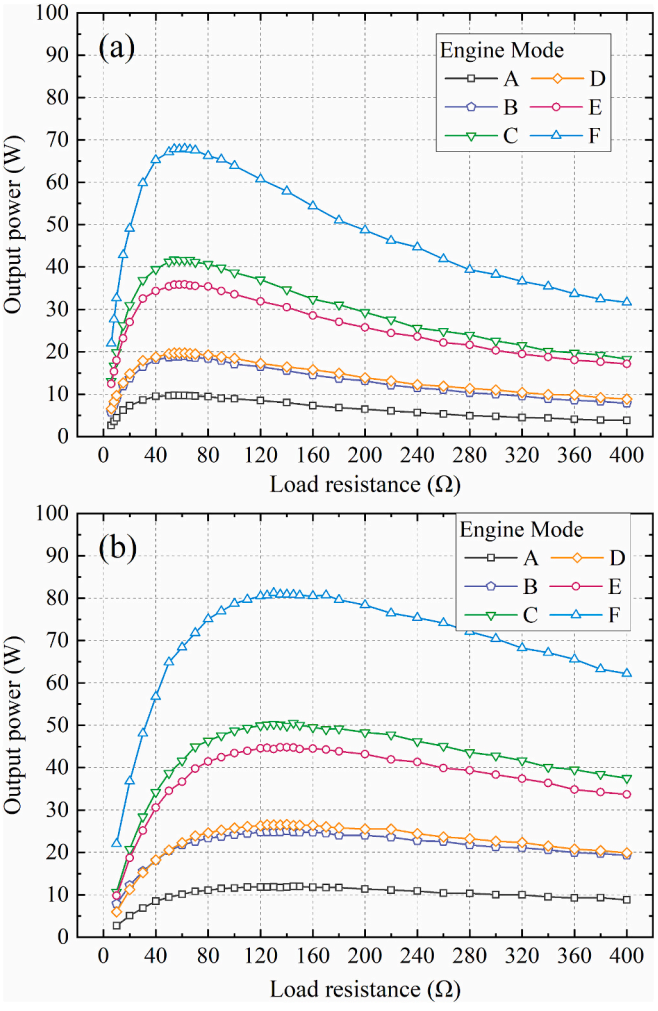

Fig. 6. Output power vs. load resistance curves of (a) Single-stage TEG and (b) Two-stage TEG under different engine modes.

marginal increase with the rise in intake temperature and flow, its impact on the optimal load is relatively modest. This proves advantageous for two-stage TEG applications, signifying that when the generator functions as an external power source, frequent adjustments to external resistance are unnecessary, ensuring that the output power remains close to its maximum value [47].

The optimum load resistance for the single-stage TEG is 62 Ω, while for the two-stage TEG, it is 136 Ω. Despite the doubling of thermoelectric legs in the two-stage TEG compared to the single-stage TEG, the optimal load resistance is not twice that of the single-stage TEG. This disparity arises because in the two-stage TEG, the average operating temperature of the TEMs is lower. This, coupled with the dual effects of the high resistivity of semiconductor materials at low temperatures and the mismatch in internal resistance caused by the series connection of 24 two-stage thermoelectric modules, leads to the optimal load resistance for the two-stage TEG being 2.2 times that of the single-stage TEG.

In theory, the matched load resistance equals the internal resistance of the TEMs [48]. In contrast to these ideal conditions, this study measured output power considering mismatches in resistance and thermal resistance between 24 single-stage and two-stage TEGs, as well as power losses caused by lead connections and uneven surface temperatures. Consequently, the optimal load resistance does not align perfectly with the internal resistance provided by the supplier.

Fig. 7(a) contrasts the thermoelectric conversion efficiency and heat recovery efficiency of single-stage and two-stage TEGs under different operating conditions. The results indicate that the two-stage TEG exhibits a slightly higher thermoelectric conversion efficiency than the single-stage TEG, with the maximum conversion efficiencies reaching 1.9% and 2.6% for single and two-stage TEG under various conditions.

As the engine speed and load increase, the thermoelectric conversion efficiency also rises, but there is a declining trend in heat recovery performance. This is due to the fact that the actual energy extraction rate increases by a magnitude smaller than the maximum possible energy extraction rate. Both single and two-stage TEGs exhibit similar trends in heat recovery performance. At the lowest engine speed and load conditions, the heat recovery efficiency is maximal, reaching 36.3% and 35% for single and two-stage TEGs, respectively. However, at the highest engine speed and load conditions, the heat recovery efficiency decreases to 26.3% and 24.6% for single and two-stage TEGs. The heat recovery performance limits the maximum output power of the TEG.

This can be elucidated by examining the temperature differentials at the inlet and outlet of the TEG based on the exhaust. Fig. 7(b) delineates the exhaust gas temperatures at the inlet and outlet of the TEG, as well as the temperature differential, under various engine operating modes. It is distinctly observable that, with the augmentation of engine speed and load, the temperature differential increases, albeit with a discernible trend of diminishing increments. A comparative analysis of diverse engine conditions reveals that this phenomenon stems from the fact that, despite the elevated intake temperature and mass flow rate accompanying the escalation of engine speed and load, the rapid flow velocity results in the exhaust gases bypassing the TEG without undergoing sufficient convective heat exchange with the TEMs, thereby flowing directly out of the TEG through smooth channel.

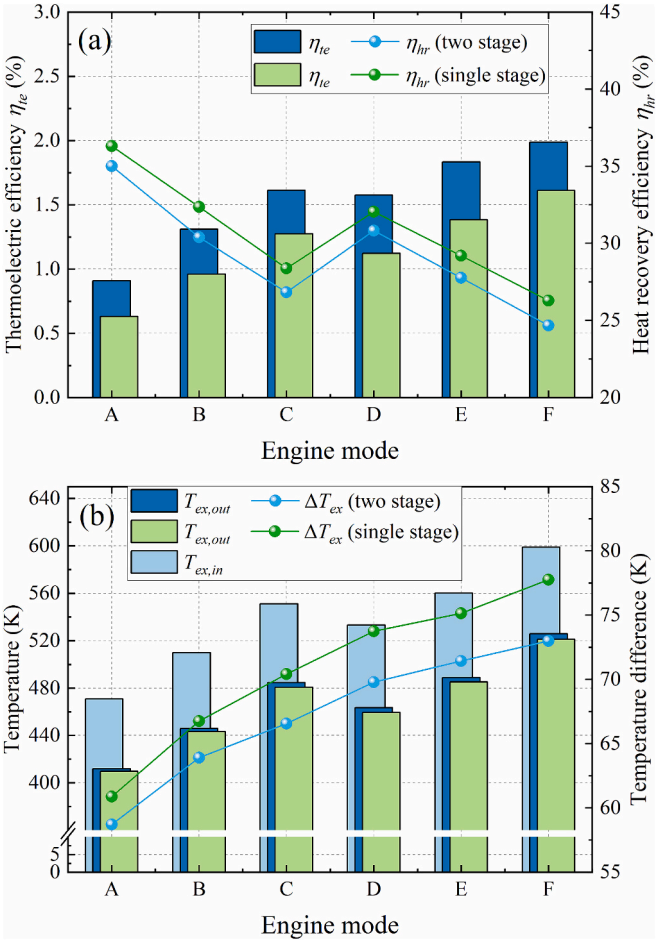

Fig. 7. Comparison of (a) Thermoelectric conversion efficiency and heat recovery efficiency and (b) inlet/outlet temperatures and temperature differences between single-stage TEG and two-stage TEG.

3.2. Influence of tape pitch ratio

The two-stage TEG manifest a notable potential for high power density in thermal energy recovery [49]. An examination was conducted on the influence of employing twisted tape heat exchangers on the performance of the two-stage TEG. Initially, an investigation was carried out on the impact of the tape pitch ratio (PR) on the thermoelectric performance of the two-stage TEG. In the experiments, the PR was set at 3, 2, 1.5, 1.2, and 1, with a twist ratio of π. As depicted in Fig. 8(a), the variation of output power with engine modes under different PR is illustrated. The insertion of twisted tapes exhibits an augmentation of thermoelectric performance. In comparison to smooth channels, the utilization of twisetd tapes at a filling ratio of PR = 1, TR = π, can potentially double the output power. Moreover, as the engine operating conditions intensify, the increase in output power becomes more substantial. This arises from the elongation of the flow path by the twisted tapes, prolonging the contact time between the fluid and the tube wall, ensuring their thorough interaction. Furthermore, the twisted tapes induce secondary flows, segregating and obstructing fluid flow, thereby accelerating the mixing velocity of fluid in the near-wall region and increasing the flow velocity near the wall [27].

As the pitch ratio diminishes, the TEG output power increases. A smaller tape gap gives rise to multiple swirling flows with greater intensity, leading to more chaotic fluid mixing and increased turbulent kinetic energy. Consequently, a smaller gap provides a thinner thermal boundary layer. This enhanced momentum transfer increases the heat extracted from the hot gas, ultimately raising the temperature on the TEG's hot side, resulting in higher power output.

The disturbances caused by the twisted tapes not only impact heat transfer but also influence the friction between the channel surface and the fluid. The increased channel area blocked by the twisted tapes and in contact with the fluid contributes to pressure loss. As shown in Fig. 8(b), under different PR, the pressure drop varies with engine modes. It is observable that as the PR decreases, the increase in pressure drop is more pronounced compared to the increase in power, reaching a maximum 6.74-fold increase over smooth pipes. This is attributed to the minimal PR signifying a heat exchanger filled with twisted tapes, resulting in more complex fluid flow and higher flow resistance.

Fig. 8(c) illustrates the impact of PR on the net output power under

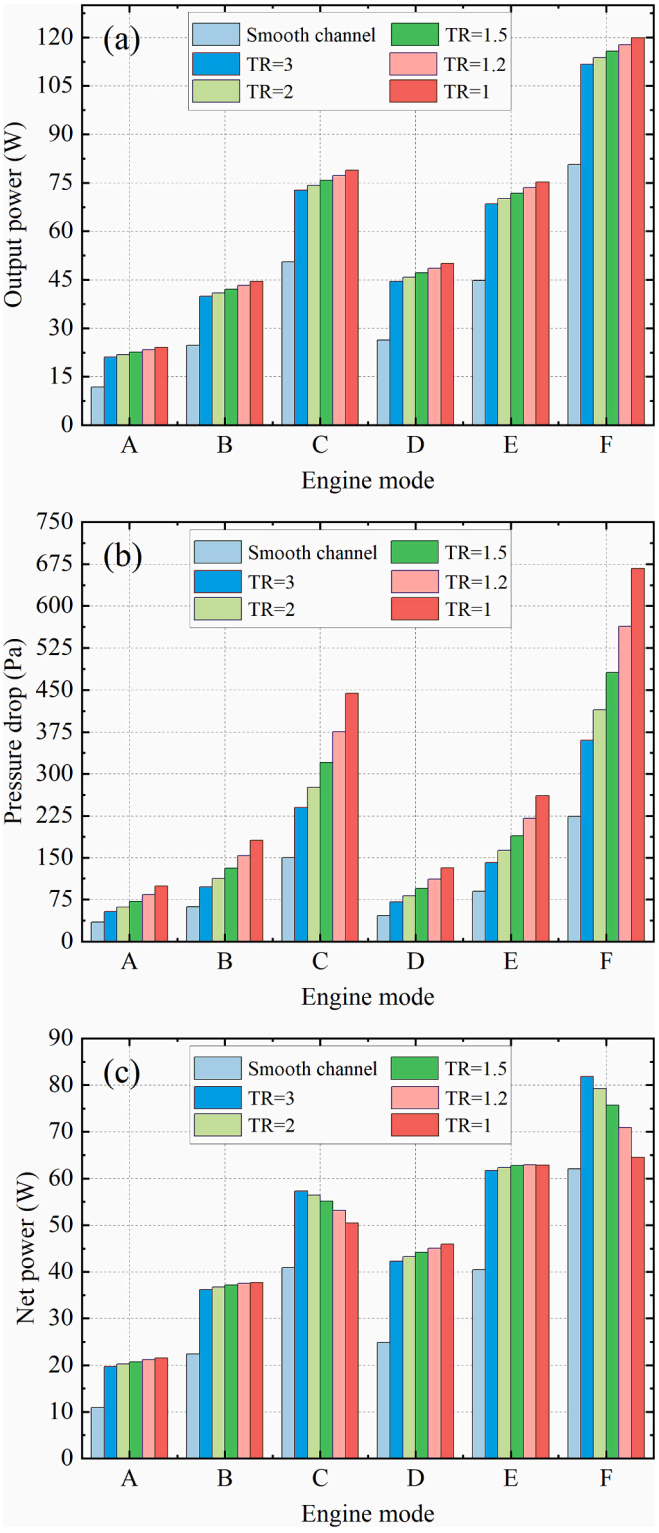

Fig. 8. Influence of different tape pitch ratios on two-stage TEG performance under various engine modes: (a) Output power, (b) Pressure drop, and (c) Net power.

various engine operating conditions. Net power reflects the coupled influence of enhanced heat transfer and frictional losses due to the twisted tapes on TEG performance. It is evident that for different engine conditions, net power exhibits distinct trends. At lower engine speeds, net power increases with decreasing PR, albeit with a diminishing rate of increase. For engine conditions A, B, D, and E, net power is nearly equivalent at tape pitch ratios of 1.5, 1.2, and 1. As engine speed increases (engine conditions C and F), the substantial increase in exhaust flow leads to a considerable rise in channel pressure drop, causing net power to decrease with decreasing PR.

3.3. Influence of twist ratio

The investigation delves into the impact of constant twist ratio and variable twist ratio twisted tapes on the output characteristics and pressure drop of the two-stage TEG system. Fig. 9a illustrates the variation of output power under different operating conditions for twisted tapes with PR = 1.5, employing constant, decreasing, and increasing twist ratios. For a uniform pitch, the output power increases with a decrease in the twist ratio. This is attributed to the enhanced convective heat transfer with a diminishing TR. Across various operating conditions, the output power with TR = π is maximized, exhibiting a 21% improvement over the twisted tape with TR = 3π. The smaller TR results in a greater number of helices, generating stronger swirling flows and higher turbulence intensity, thereby achieving superior heat transfer. As the exhaust temperature and flow rate decrease, the enhancement ratio of output power with TR = π compared to TR = 3π declines from 21% to 16%, owing to the superior thermal performance of twisted tapes at low Reynolds numbers [30].

For a typical twisted tape, the thermodynamic properties vary with the degree of looseness of the tape. Larger TR leads to a looser configuration, and vice versa. According to Fig. 9, the DTR-TT of TR = 3π to π is tighter than that of TR = 3π to 2π, so the output power is greater. The DTR-TT with TR = 3π to π exhibits greater output power than the CTR-TT with TR = 3π, yet less than the twisted tape with TR = π. However, it surpasses the output power of the average TR = 2π twisted tape, indicating the enhanced heat transfer performance of variable twist ratio TTs compared to constant twist ratio TTs.

Under the same variable twist ratio combination, the output power of

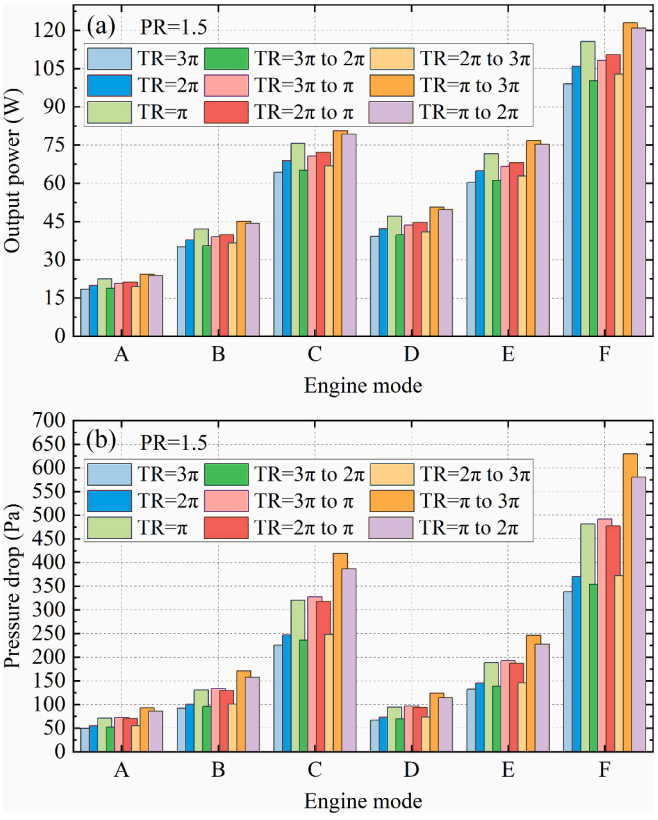

Fig. 9. Output power and pressure drop of constant and variable twist ratios under different engine modes.

the ITR-TT is consistently higher than that of DTR-TT. For instance, in engine mode F, the output power of TR = π to 3π ITR-TT is 25% higher than that of TR = 3π to π DTR-TT. This is attributed to the lower pressure drop upstream in general pipes, resulting in lower pressure loss and higher temperature gradients. The addition of ITR-TT increases the number and intensity of swirls upstream, yielding superior heat transfer performance. Therefore, twisted tapes with shorter twist lengths inserted upstream in the pipe achieve higher TEG output power.

An noteworthy observation is that the output power of TR = π to 3π ITR-TT is higher than that of TR = π to 2π ITR-TT. The looser variable twist ratio TT enables TEG to attain better output performance, in contrast to the pattern observed with DTR-TT. This is because the non-uniform distribution of the internal vortex flow field in TR = π to 3π ITR-TT (VTR = 1/3) is more pronounced than that in TR = π to 2π ITR-TT (VTR = 1/2). This non-uniform distribution generates a larger effective driving potential induced by the twisted tape than the one induced by a uniform tape, resulting in higher heat and momentum fluxes. Hence, for increasing twist ratio twisted tapes, the influence of flow instability is more significant than the influence of swirl intensity. Expanding the pitch variation range of variable twist ratio TTs can enhance heat transfer performance.

Fig. 9(b) illustrates the variation in pressure drop under different

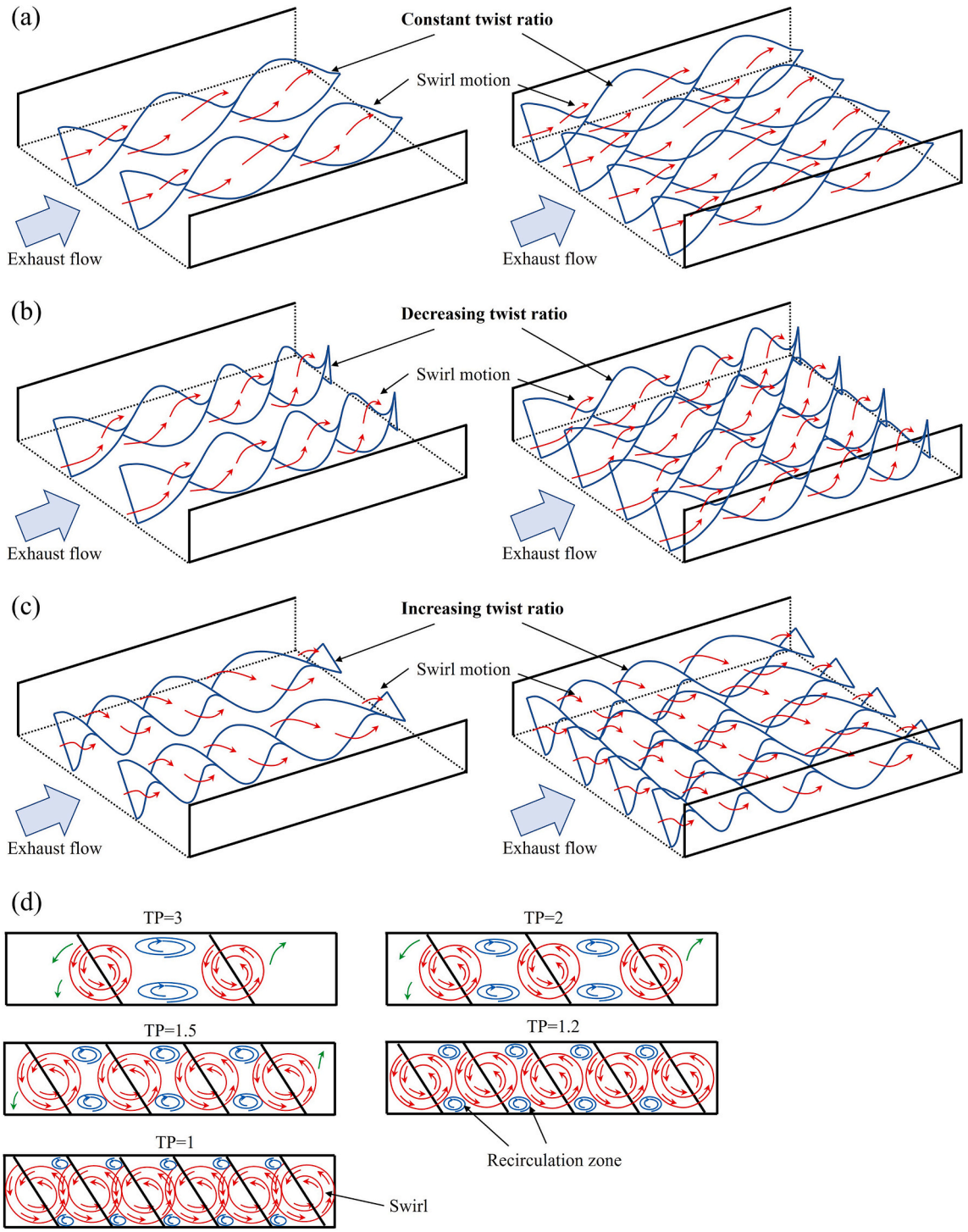

Fig. 10. Theoretical flow patterns under different TR and PR.

operating conditions for CTR, DTR, and ITR twisted tapes. The trend in pressure drop mirrors the trend in TEG output power, as the effect of enhanced heat transfer is accompanied by an increase in friction coefficient. The noteworthy difference is that, for DTR-TT, the impact of flow instability on pressure drop is greater than its impact on heat transfer performance. The output power and pressure drop of TR = 3π to π DTR-TT are 2.5% lower and 3.2% higher, respectively, compared to those of TR = 2π to π DTR-TT. The flow patterns depicted in Fig. 10 aid in understanding the influence of twist ratio and tape pitch ratio on fluid flow and heat transfer mechanisms within the heat exchanger channels in this study [50].

3.4. Net power analysis

The enhanced heat transfer effectiveness of variable twist ratio twisted tapes surpasses that of typical twisted tapes, but the resulting additional pressure drop is also significantly higher. Once the engine back pressure exceeds a certain level, it not only affects the normal operation of the engine but also leads to an increase in resistance power consumption, potentially surpassing the output power generated by the TEG itself [51]. To assess the overall performance of variable twist ratio twisted tapes in the TEG system, the impact of different variable twist ratio TT on the net output power of the TEG was evaluated.

Fig. 11(a), (b), and (c) depict the variation in net output power for TEGs employing CTR, DTR, and ITR twisted tapes with PR = 1.5 under different operating conditions. For CTR-TT, the net power increases with a decrease in TR. However, for DTR-TT, the tape with the highest rate of TR variation results in lower net power, particularly at high engine speeds. This indicates that the flow instability of DTR-TT leads to inferior overall performance compared to typical tapes, corroborating the conclusions from Fig. 9. In contrast, increasing twist ratio twisted tape yields different results. In most operating conditions, TR = π to 3π ITR-TT achieves the best thermoelectric performance. In mode D, the net output power of TR = π to 3π ITR-TT is 5.9% and 17.1% higher than that of CTR-TT with twist ratios of π and 2π, respectively.

Fig. 11(d), (e), and (f) illustrate the variation in net thermoelectric efficiency ($\eta_{net} = P_{net}/Q_h$) for TEGs employing CTR, DTR, and ITR twisted tapes with PR = 1.5 under different operating conditions. The trend in net efficiency follows a similar pattern to net power. The net efficiency of ITR-TT is superior to CTR-TT at low engine speeds and comparable at high engine speeds. From an efficiency standpoint, ITR-TT also represent the most effective enhancement for thermoelectric performance.

To accentuate the advantages of variable twist ratio twisted tapes, Fig. 12 compares the ratio of the net power of the TEG system after enhanced heat transfer to the net power of the TEG system before

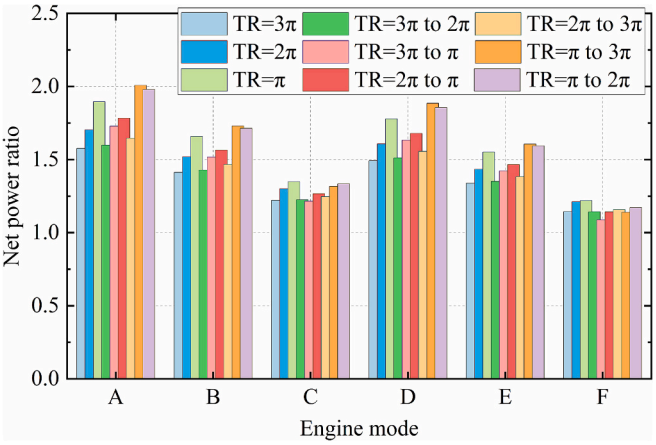

Fig. 12. Net power ratio of two-stage TEG with twisted tape heat exchanger and two-stage TEG with smooth heat exchanger.

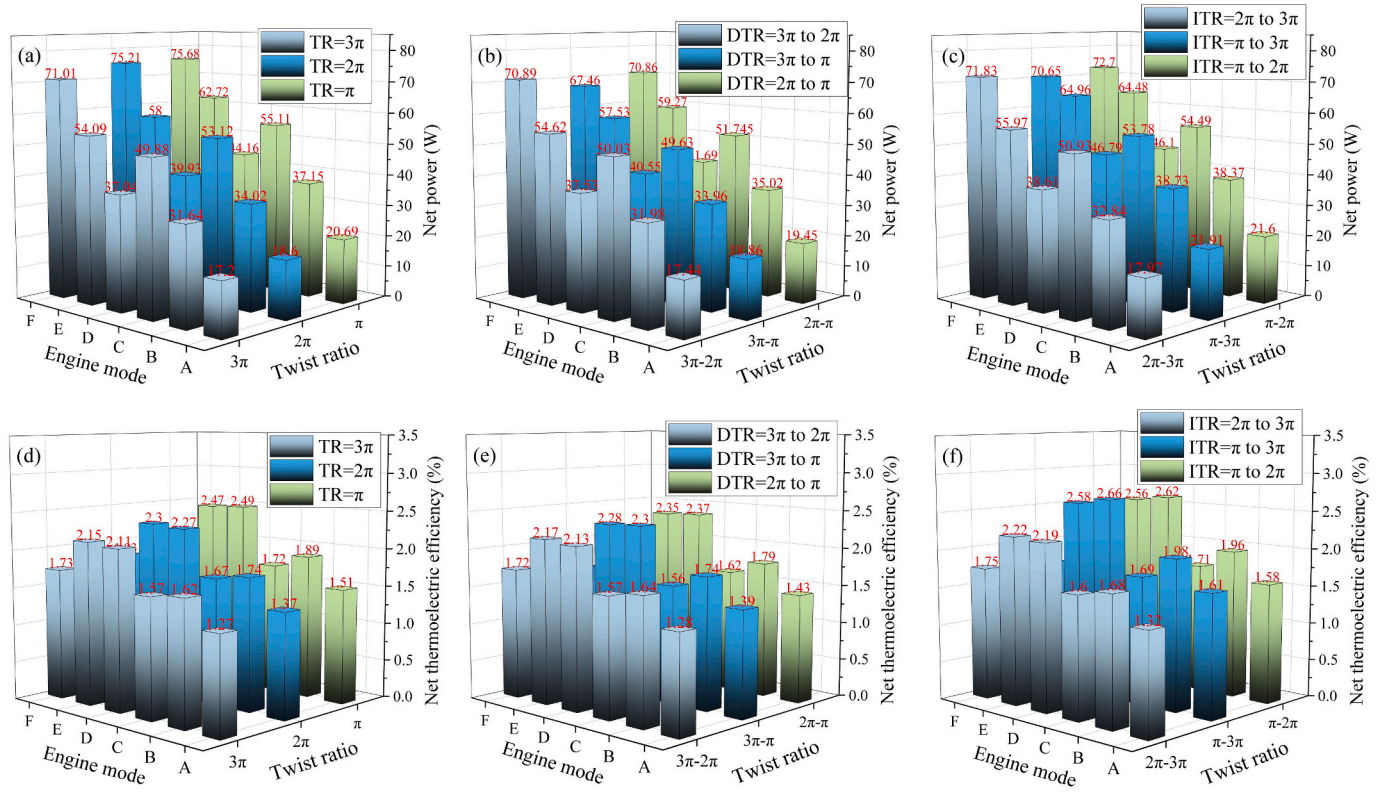

Fig. 11. Net power of (a) Constant twist ratio, (b) Decreasing twist ratio, and (c) Increasing twist ratio under different engine modes; as well as net conversion efficiency of (a) Constant twist ratio, (b) Decreasing twist ratio, and (c) Increasing twist ratio under different engine modes.

enhanced heat transfer [52]. This ratio characterizes the enhancement in overall TEG performance relative to smooth heat exchanger. As engine speed and load increase, the net power enhancement ratio of twisted tape decreases. In engine mode A, twisted tapes with twist ratios of 3π, 2π, π, 3π-2π, 3π-π, 2π-π, 2π-3π, π-3π, and π-2π yield net power enhancements of 57.7%, 70.5%, 89%, 60%, 72.8%, 78.3%, 64.7%, 100%, and 98%, respectively, compared to a regular smooth heat exchanger. Except for engine mode F, the enhancement ratio of TR = π to 3π ITR-TT is superior to that of CTR-TT and DTR-TT in other operating conditions.

Finally, to highlight the novelty and advancement of this study, we compare the two-stage TEG with the optimal variable twist ratio twisted tapes to a typical TEG without heat transfer optimization, as shown in Fig. 13. The typical TEG employs commercially available single-stage thermoelectric modules and is equipped with a smooth flat-plate heat exchanger. In the two-stage TEG, the two-stage TEMs developed in Section 2.1 are utilized, and TR = π to 3π variable twist ratio twisted tapes with a tape pitch ratio of 1.5 are inserted into the heat exchanger, as discussed in Section 2.1.

It is evident that, through the optimization of thermoelectric modules and heat transfer performance on the hot side, the overall performance of the TEG has been significantly enhanced, despite the increase in exhaust pressure drop. Although the pressure drop has increased by 1.5 times, the output power, net power, thermoelectric conversion efficiency, heat recovery efficiency, and net efficiency have all improved by approximately double. It is worth noting that if the issue of internal resistance mismatch in the two-stage thermoelectric modules is addressed, and compatibility with various thermoelectric materials is achieved for the temperature gradient, the comprehensive performance of the TEG will see further substantial improvement. This will be pursued in our future research endeavors. As the cost of thermoelectric modules continues to decrease, there is a potential for the power-to-cost ratio of two-stage thermoelectric generators to surpass that of single-stage thermoelectric generators.

4. Conclusions

In this study, we conducted a comprehensive examination of the experimental system for a exhaust heat recovery thermoelectric generator, comparing the thermoelectric characteristics of single-stage and two-stage generators. Additionally, we introduced a method to enhance heat transfer through the utilization of variable twist ratio twisted tapes and systematically investigated its impact on the performance of the two-stage thermoelectric generator. From our research findings, the following conclusions can be drawn:

1. In comparison to a single-stage thermoelectric generator, under engine mode F, the two-stage thermoelectric generator leads to a 17.3% increase in output power, and the optimum load resistance is enhanced by approximately 2.2 times.
2. The output power and pressure drop of the two-stage thermoelectric generator both increase with a decrease in tape pitch ratio, with the pressure drop increase being more pronounced. Compared to a smooth heat exchanger, the minimum tape pitch ratio results in a 6.74-fold increase in pressure drop. At low engine speeds and loads, a smaller tape pitch ratio yields higher net output power, while at high engine speeds and loads, net power decreases with a decrease in tape pitch ratio.
3. Output power and pressure drop increase with a decrease in twist ratio. Due to the more significant influence of flow instability compared to swirl intensity, the output power of the twisted tape with an increased twist ratio from π to 3π is 25% higher than that of the twisted tape with a twist ratio increased from π to 2π.
4. The increasing twist ratio twisted tape with the highest twist ratio variation rate exhibits the highest net output power. Under engine operating condition A, the net output power gain can reach a maximum of 100% compared to the unmodified thermoelectric generator.

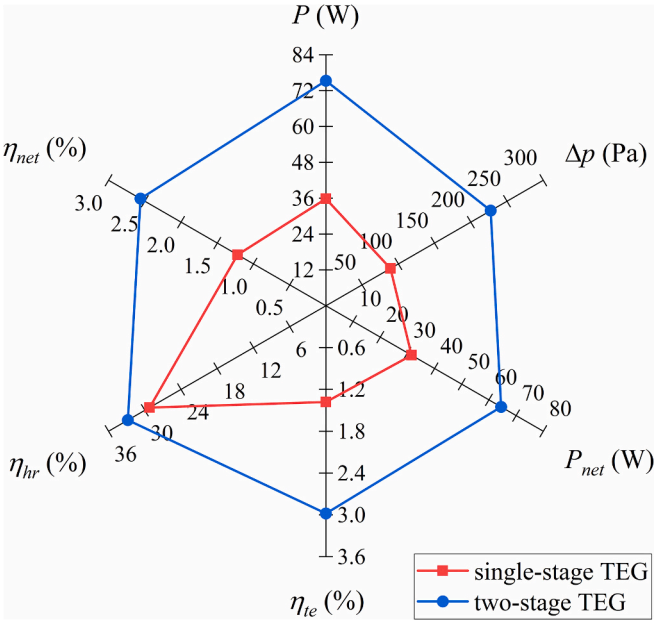

Fig. 13. Comparison of thermoelectric performance between single-stage TEG with smooth heat exchanger and two-stage TEG with ITR-TT heat exchanger under engine mode E.

CRediT authorship contribution statement

Wenlong Yang: Conceptualization, Data curation, Writing – original draft. **Chenchen Jin:** Investigation, Writing – original draft. **Wenchao Zhu:** Methodology, Software, Validation. **Changjun Xie:** Funding acquisition, Project administration, Resources, Writing – review & editing. **Liang Huang:** Formal analysis, Software, Visualization. **Yang Li:** Supervision, Validation, Writing – review & editing. **Binyu Xiong:** Formal analysis, Methodology, Writing – review & editing.

Declaration of competing interest

The authors declare that they have no known competing financial interests or personal relationships that could have appeared to influence the work reported in this paper.

Data availability

Data will be made available on request.

Acknowledgments

This work is supported by the National Natural Science Foundation of China (51977164) and the Postdoctoral Fellowship Program of CPSF (GZC20232011).

References

[1] He J, Li K, Jia L, Zhu Y, Zhang H, Linghu J. Advances in the applications of thermoelectric generators. Appl Therm Eng 2024;236:121813. https://doi.org/10.1016/j.applthermaleng.2023.121813.
[2] Burnete NV, Mariasiu F, Depcik C, Barabas I, Moldovanu D. Review of thermoelectric generation for internal combustion engine waste heat recovery. Prog Energ Combust 2022;91:101009. https://doi.org/10.1016/j.pecs.2022.101009.
[3] Saha M, Tregenza O, Twelftree J, Hulston C. A review of thermoelectric generators for waste heat recovery in marine applications. Sustain Energy Technol Assess 2023;59:101684. https://doi.org/10.1016/j.seta.2023.103394.

[4] Waseem M, Amir M, Lakshmi GS, Harivardhagini S, Ahmad M. Fuel cell-based hybrid electric vehicles: an integrated review of current status, key challenges, recommended policies, and future prospects. Green Energy Intell Transp 2023;2(6):100121. https://doi.org/10.1016/j.geits.2023.100121.

[5] Ochieng AO, Megahed TF, Ookawara S, Hassan H. Comprehensive review in waste heat recovery in different thermal energy-consuming processes using thermoelectric generators for electrical power generation. Process Saf Environ 2022;162:134–54. https://doi.org/10.1016/j.psep.2022.03.070.

[6] Liu X, Deng YD, Li Z, Su CQ. Performance analysis of a waste heat recovery thermoelectric generation system for automotive application. Energ Conver Manage 2015;90:121–7. https://doi.org/10.1016/j.enconman.2014.11.015.

[7] Zhang Y, Cleary M, Wang X, Kempf N, Schoensee L, Yang J, et al. High-temperature and high-power-density nanostructured thermoelectric generator for automotive waste heat recovery. Energ Conver Manage 2015;105:946–50. https://doi.org/10.1016/j.enconman.2015.08.051.

[8] Zhu W, Yang W, Yang Y, Li Y, Li H, Shi Y, et al. Economic configuration optimization of onboard annual thermoelectric generators under multiple operating conditions. Renew Energy 2022;197:486–99. https://doi.org/10.1016/j.renene.2022.07.124.

[9] Ying P, He R, Mao J, Zhang Q, Reith H, Sui J, et al. Towards tellurium-free thermoelectric modules for power generation from low-grade heat. Nat Commun 2021;12:1121. https://doi.org/10.1038/s41467-021-21391-1.

[10] Alghamdi H, Maduabuchi C, Okoli K, Albaker A, Alanazi M, Alghassab M, et al. From sunlight to power: enhancing 4E performance with two-stage segmented thermoelectric generators in concentrated solar applications. J Clean Prod 2023;429:139314. https://doi.org/10.1016/j.jclepro.2023.139314.

[11] Cózar IR, Pujol T, Lehocky M. Numerical analysis of the effects of electrical and thermal configurations of thermoelectric modules in large-scale thermoelectric generators. Appl Energy 2018;229:264–80. https://doi.org/10.1016/j.apenergy.2018.07.116.

[12] Yang W, Jin C, Zhu W, Li Y, Zhang R, Huang L, et al. Taguchi optimization and thermoelectrical analysis of a pin fin annular thermoelectric generator for automotive waste heat recovery. Renew Energy 2024;220:119628. https://doi.org/10.1016/j.renene.2023.119628.

[13] Yang W, Zhu W, Yang Y, Huang L, Shi Y, Xie C. Thermoelectric performance evaluation and optimization in a concentric annular thermoelectric generator under different cooling methods. Energies 2022;15:2231. https://doi.org/10.3390/en15062231.

[14] Li G, Ying J, Zheng Y, Guo W, Tang Y, Ye C. Analytical design model for waste heat thermoelectric generator and experimental verification. Energ Conver Manage 2022;252:115034. https://doi.org/10.1016/j.enconman.2021.115034.

[15] Zhao Y, Li W, Zhao X, Wang Y, Luo D, Li Y, et al. Energy and exergy analysis of a thermoelectric generator system for automotive exhaust waste heat recovery. Appl Therm Eng 2024;239:122180. https://doi.org/10.1016/j.applthermaleng.2023.122180.

[16] Luo D, Yan Y, Chen W-H, Yang X, Chen H, Cao B, et al. A comprehensive hybrid transient CFD-thermal resistance model for automobile thermoelectric generators. Int J Heat Mass Transf 2023;211:124203. https://doi.org/10.1016/j.ijheatmasstransfer.2023.124203.

[17] He M, Wang E, Zhang Y, Zhang W, Zhang F, Zhao C. Performance analysis of a multilayer thermoelectric generator for exhaust heat recovery of a heavy-duty diesel engine. Appl Energy 2020;274:115298. https://doi.org/10.1016/j.apenergy.2020.115298.

[18] Pujol T, Jollyn IT, Massaguer E, Massaguer A, Cózar IR, Paepe MD. Design optimization of plate-fin heat sink with forced convection for single-module thermoelectric generator. Appl Therm Eng 2023;221:119866. https://doi.org/10.1016/j.applthermaleng.2022.119866.

[19] Chen W-H, Wang C-M, Saw LH, Hoang AT, Bandala AA. Performance evaluation and improvement of thermoelectric generators (TEG): fin installation and compromise optimization. Energ Conver Manage 2021;250:114858. https://doi.org/10.1016/j.enconman.2021.114858.

[20] Zhao Y, Lu M, Li Y, Wang Y, Ge M. Numerical investigation of an exhaust thermoelectric generator with a perforated plate. Energy 2023;263:125776. https://doi.org/10.1016/j.energy.2022.125776.

[21] Buononmo B, Cascetta F, Pasqua AD, Manca O. Performance parameters enhancement of a thermoelectric generator by metal foam in exhaust automotive lines. Therm Sci Eng Prog 2023;38:101684. https://doi.org/10.1016/j.tsep.2023.101684.

[22] Li Y, Wang S, Zhao Y, Yue L. Effect of thermoelectric modules with different characteristics on the performance of thermoelectric generators inserted in the central flow region with porous foam copper. Appl Energy 2022;327:120041. https://doi.org/10.1016/j.apenergy.2022.120041.

[23] He W, Guo R, Takasu H, Kato Y, Wang S. Performance optimization of common plate-type thermoelectric generator in vehicle exhaust power generation systems. Energy 2019;175:1153–63. https://doi.org/10.1016/j.energy.2019.03.174.

[24] Luo D, Wang R, Yu W, Zhou W. A numerical study on the performance of a converging thermoelectric generator system used for waste heat recovery. Appl Energy 2020;270:115181. https://doi.org/10.1016/j.apenergy.2020.115181.

[25] Yang W, Zhu W, Li Y, Zhang L, Zhao B, Xie C, et al. Annular thermoelectric generator performance optimization analysis based on concentric annular heat exchanger. Energy 2022;239:122127. https://doi.org/10.1016/j.energy.2021.122127.

[26] Luo D, Wu Z, Yan Y, Cao J, Yang X, Zhao Y, et al. Performance investigation and design optimization of a battery thermal management system with thermoelectric coolers and phase change materials. J Clean Prod 2024;434:139834. https://doi.org/10.1016/j.jclepro.2023.139834.

[27] Eiamsa-ard S, Wongcharee K, Promvonge P. Influence of nonuniform twisted tape on heat transfer enhancement characteristics. Chem Eng Commun 2012;199(10):1279–97. https://doi.org/10.1080/00986445.2012.668724.

[28] Bucak H, Yılmaz F. The current state on the thermal performance of twisted tapes: a geometrical categorisation approach. Chem Eng Process 2020;153:107929. https://doi.org/10.1016/j.cep.2020.107929.

[29] Zhu W, Xu A, Yang W, Xiong B, Xie C, Li Y, et al. Optimal design of annular thermoelectric generator with twisted tape for performance enhancement. Energ Conver Manage 2022;270:116258. https://doi.org/10.1016/j.enconman.2022.116258.

[30] Varun MO, Garg H Nautiyal, Khurana S, Shukla MK. Heat transfer augmentation using twisted tape inserts: a review. Renew Sustain Energy Rev 2016;63:193–225. https://doi.org/10.1016/j.rser.2016.04.051.

[31] Karana DR, Sahoo RR. Performance assessment of the automotive heat exchanger with twisted tape for thermoelectric based waste heat recovery. J Clean Prod 2021;283:124631. https://doi.org/10.1016/j.jclepro.2020.124631.

[32] Demeke W, Ryu B, Ryu S. Machine learning-based optimization of segmented thermoelectric power generators using temperature-dependent performance properties. Appl Energy 2024;355:122216. https://doi.org/10.1016/j.apenergy.2023.122216.

[33] Erro I, Aranguren P, Alzuguren I, Chavarren D, Astrain D. Experimental analysis of one and two-stage thermoelectric heat pumps to enhance the performance of a thermal energy storage. Energy 2023;285:129447. https://doi.org/10.1016/j.energy.2023.129447.

[34] Alghamdi H, Maduabuchi C, Okoli K, Albaker A, Makki E, Alghassab M, et al. Pioneering sustainable power: harnessing material innovations in double stage segmented thermoelectric generators for optimal 4E performance. Appl Energy 2023;352:121885. https://doi.org/10.1016/j.apenergy.2023.121885.

[35] Ge M, Xuan Z, Liu X, Luo D, Wang Y, Li Y. Structural optimization of solar thermoelectric generators considering thermal stress conditions. J Clean Prod 2023;428:139367. https://doi.org/10.1016/j.jclepro.2023.139367.

[36] Kim TY, Negash AA, Cho G. Waste heat recovery of a diesel engine using a thermoelectric generator equipped with customized thermoelectric modules. Energ Conver Manage 2016;124:280–6. https://doi.org/10.1016/j.enconman.2016.07.013.

[37] Lu X, Yu X, Qu Z, Wang Q, Ma T. Experimental investigation on thermoelectric generator with non-uniform hot-side heat exchanger for waste heat recovery. Energ Conver Manage 2017;150:403–14. https://doi.org/10.1016/j.enconman.2017.08.030.

[38] Ge M, Li Z, Zhao Y, Xuan Z, Li Y, Zhao Y. Experimental study of thermoelectric generator with different numbers of modules for waste heat recovery. Appl Energy 2022;322:119523. https://doi.org/10.1016/j.apenergy.2022.119523.

[39] Negash AA, Choi Y, Kim TY. Experimental investigation of optimal location of flow straightener from the aspects of power output and pressure drop characteristics of a thermoelectric generator. Energy 2021;219:119565. https://doi.org/10.1016/j.energy.2020.119565.

[40] Kim TY, Ewak J, Kim B-W. Energy harvesting performance of hexagonal shaped thermoelectric generator for passenger vehicle applications: an experimental approach. Energ Conver Manage 2018;160:14–21. https://doi.org/10.1016/j.enconman.2018.01.032.

[41] Wang T, Luan W, Liu T, Tu S-T, Yan J. Performance enhancement of thermoelectric waste heat recovery system by using metal foam inserts. Energ Conver Manage 2016;124:13–9. https://doi.org/10.1016/j.enconman.2016.07.006.

[42] Zhang H, Nunayon SS, Jin X, Lai ACK. Pressure drop and nanoparticle deposition characteristics for multiple twisted tape inserts with partitions in turbulent duct flows. Int J Heat Mass Tran 2022;193:121474. https://doi.org/10.1016/j.ijheatmasstransfer.2021.121474.

[43] Yang W, Zhu W, Du B, Wang H, Xu L, Xie C, et al. Power generation of annular thermoelectric generator with silicone polymer thermal conductive oil applied in automotive waste heat recovery. Energy 2023;282:128400. https://doi.org/10.1016/j.energy.2023.128400.

[44] Yang W, Zhu W, Li Y, Xie C, Xiong B, Shi Y, et al. Global structural optimization of annular thermoelectric generators based on a dual-finite-element multiphysical model. Appl Therm Eng 2023;220:119797. https://doi.org/10.1016/j.applthermaleng.2022.119797.

[45] Xuan Z, Ge M, Zhao C, Li Y, Wang S, Zhao Y. Effect of nonuniform solar radiation on the performance of solar thermoelectric generators. Energy 2024;290:130249. https://doi.org/10.1016/j.energy.2024.130249.

[46] Zhao X, Jiang J, Zuo H, Mao Z. Performance analysis of diesel particulate filter thermoelectric conversion mobile energy storage system under engine conditions of low-speed and light-load. Energy 2023;282:128411. https://doi.org/10.1016/j.energy.2023.128411.

[47] Yang W, Xu A, Zhu W, Li Y, Shi Y, Huang L, et al. Performance improvement and thermomechanical analysis of a novel asymmetrical annular thermoelectric generator. Appl Therm Eng 2024;237:121804. https://doi.org/10.1016/j.applthermaleng.2023.121804.

[48] Zhu W, Weng Z, Li Y, Zhang L, Zhao B, Xie C, et al. Theoretical analysis of shape factor on performance of annular thermoelectric generators under different thermal boundary conditions. Energy 2022;239:122285. https://doi.org/10.1016/j.energy.2021.122285.

[49] Yin T, Li Z-M, Peng P, Liu W, Shao Y-Y, He Z-Z. Performance analysis of a novel two-stage automobile thermoelectric generator with the temperature-dependent materials. Appl Therm Eng 2021;195:117249. https://doi.org/10.1016/j.applthermaleng.2021.117249.

[50] Vashistha C, Patil AK, Kumar M. Experimental investigation of heat transfer and pressure drop in a circular tube with multiple inserts. Appl Therm Eng 2016;96:117–29. https://doi.org/10.1016/j.applthermaleng.2015.11.077.
[51] Luo D, Yan Y, Li Y, Yang X, Chen H. Exhaust channel optimization of the automobile thermoelectric generator to produce the highest net power. Energy 2023;281:128319. https://doi.org/10.1016/j.energy.2023.128319.
[52] Yang Y, Wang S, Zhu Y. Evaluation method for assessing heat transfer enhancement effect on performance improvement of thermoelectric generator systems. Appl Energy 2020;263:114688. https://doi.org/10.1016/j.apenergy.2020.114688.